ACS NANO
Cite This: ACS Nano 2019, 13, 582−590
www.acsnano.org

ARTICLE

Static and Dynamic Piezopotential Modulation in Piezo-Electret Gated MoS_2 Field-Effect Transistor

Jing Zhao,[†] Zheng Wei,[‡] Qian Zhang,[†] Hua Yu,[‡] Shuopei Wang,[‡] Xixi Yang,[†] Guoyun Gao,[†] Shanshan Qin,[†] Guangyu Zhang,*[,‡,§] Qijun Sun,*[,†,∥] and Zhong Lin Wang*[,†,∥,⊥]

[†]Beijing Institute of Nanoenergy and Nanosystems, Chinese Academy of Sciences, Beijing 100083, China
[‡]Beijing National Laboratory for Condensed Matter Physics and Institute of Physics, Chinese Academy of Sciences, Beijing 100190, China
[∥]Center on Nanoenergy Research, School of Physical Science and Technology, Guangxi University, Nanning 530004, China
[§]Collaborative Innovation Center of Quantum Matter, Beijing Key Laboratory for Nanomaterials and Nanodevices, Beijing 100190, China
[⊥]School of Materials Science and Engineering, Georgia Institute of Technology, Atlanta, Georgia 30332-0245, United States

Supporting Information

ABSTRACT: The piezotronic effect links the mechanical stimuli with various semiconductor devices, promising for low-power-consuming electronic devices, sensitive sensors, and interactive control systems. The persistent requirement for external strains in piezotronic modulation may hinder its application in some circumstances (such as devices on rigid substrate or complicated synergistic piezoelectric modulation on multidevice). Here, we propose an efficient method to realize piezoelectric modulation of optical and electrical properties of MoS_2 FET in both static and dynamic manner, expanding the application of piezotronics. Through capacitive coupling between piezo-electret and MoS_2 FET, the remanent piezopotential can efficiently tune the Fermi level of MoS_2, programming the initial electrical property for subsequent fabrication of sophisticated devices. The external strain can induce enhanced piezo-potentials to further affect the energy band bending of MoS_2 channel, giving rise to high-performance strain sensors (large gauge factor ~4800, fast response time ~0.15 s, and good durability >1000 s). The proposed static and dynamic piezopotential tuned MoS_2 FET is easy to extend to devices based on other materials, which is highly desired in tunable sensory systems, active flexible electronics, and human−machine interface.

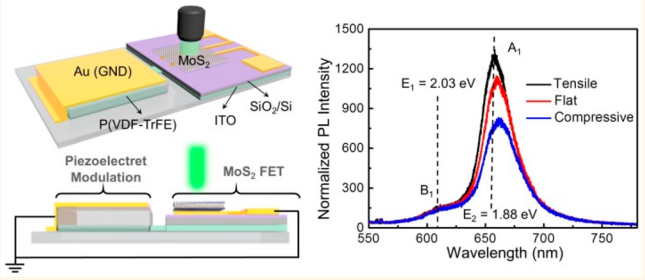

KEYWORDS: *piezopotential modulation, MoS_2 FET, optical and electric properties, piezo-electret, mechanical sensors*

Piezotronic effect is to use the piezoelectric polarization charges to serve as a "gate" for controlling the transport in semiconductors, especially at a metal−semiconductor contact (M−S contact) or p−n junction.[1,2] It is highly desirable and compatible in ultrasensitive nanoforce sensors and biosensors, high-resolution adaptive sensing arrays, piezotronic transistors, and optoelectronic device modulations.[3−6] Piezopotential is an intrinsic inner-crystal field induced by electric dipole moments, which is originated from nonmobile ions on crystal lattice sites or polar molecular groups with asymmetric charge surroundings. Therefore, piezopotential can be maintained as long as the piezoelectric material is subjected to external strains, that is, piezoelectric polarization requires persistent external strain. As the piezopotential is in linear dependence with applied strain, the piezoelectric effect is beneficial for the dynamic response of the piezotronic devices, such as mechanical sensing, actuation, interactive modulation, and energy transduction. Meanwhile, the static piezoelectric modulation of electrical properties free from external strains is also important, yet uneasy to be realized in some specific situations (such as devices on rigid substrate or multidevices operation under synergistic piezoelectric modulation). Therefore, broadening the semiconductor device modulation modes by piezo-polarization in both

Received: September 30, 2018
Accepted: December 18, 2018
Published: December 18, 2018

DOI: 10.1021/acsnano.8b07477
ACS Nano 2019, 13, 582−590

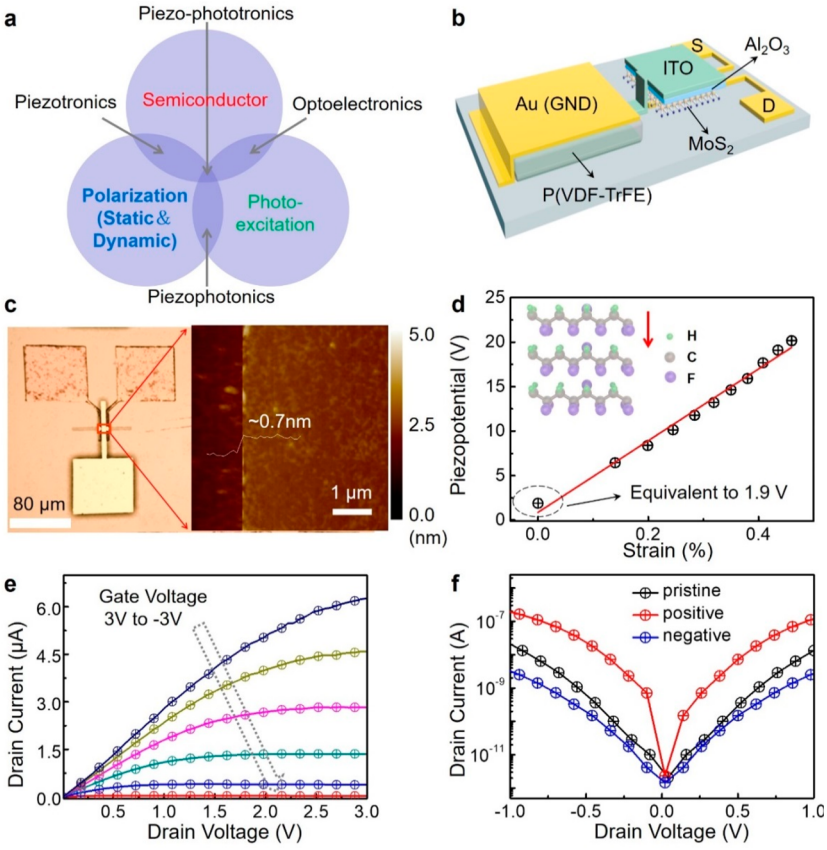

Figure 1. Static electric regulation of the MoS_2 FET by the P(VDF-TrFE) film as a gate material. (a) The schematic diagram of polarization, piezoelectricity, and semiconductor coupling. (b) The schematic diagram of the device with flexible P(VDF-TrFE) film on PET substrate. (c) The optical image of the MoS_2 pattern with source−drain electrodes (left). The right panel is the AFM image of the MoS_2 channel with a thickness of ∼0.7 nm. (d) The remanent voltage of P(VDF-TrFE) is ∼1.9 V after polarization, and the piezo-potential increases with the strain. (e) The output property of the device with channel length and width is ∼20 μm and ∼5 μm, respectively. (f) The *I*−*V* curve for the MoS_2 device gated by the P(VDF-TrFE) piezo-electret under opposite polarized voltages.

static and dynamic manner is critical from both materials and device structure aspects.[7−10]

Transition-metal dichalcogenides (TMDCs) have attracted significant attentions for soft electronics due to their excellent electrical, optical, thermal, and mechanical properties.[11−15] As a representative of TMDCs, molybdenum disulfide (MoS_2) consists of S−Mo−S sandwiched atomic units in a hexagonal-structured crystal, exhibiting a 1.9 eV direct band gap for the monolayer.[16] The mobility and on/off ratios of MoS_2 field-effect transistor (FET) can be achieved up to 1000 $cm^2 \cdot V^{-1} \cdot s^{-1}$ (at low temperature) and 10^8, respectively.[17] Its superior resistance to short-channel effects, attractive electrical performance characteristics, high electrostatic control and high surface-to-volume ratio promise wide applications for flexible optoelectronic devices, ultrasensitive sensors, supercapacitors, catalysis, *etc.*[18−25] According to the noncentral symmetry of its crystal structures, the intrinsic piezoelectricity of MoS_2 is theoretically predicted and experimentally demonstrated in the odd-layer samples by mechanical exfoliation. Piezoelectric polarization in the atomically thin semiconductor induced by external strain can control the charge carriers transport and modulate the Schottky barrier at M−S contacts, that is, piezotronic effect in 2D piezoelectric semiconductors.[26−28] However, the piezotronic modulation is elusive to achieve due to the difficulty in both accurate preparation of odd-layer MoS_2 in single crystal and construction of perfect metal contacts. The piezoresistive effect companied with mechanical strains can also change the band structure to confound with piezotronic effect, which may hinder the piezotronic modulation in sophisticated devices. Therefore, it is critical to develop a simple and universal method to achieve the facile piezoelectric modulation of 2D materials based semiconductor devices. Capacitive coupling by connecting piezoelectric materials and semiconductor devices in series offers an alternative way to control the charge transport in semiconductor devices.[29−32] Different types of piezoelectric materials (such as piezo-electrets, piezoelectric, and ferroelectric materials) are facile to be integrated to realize efficient piezoelectric modulation, which can complement and expand the application of piezotronics.[33−35]

In this work, a piezo-electret polymer was capacitively coupled with MoS_2 FET to achieve both static and dynamic piezoelectric tuning of the transport properties. On one hand, the remnant polarization induced by aligned dipoles in a piezo-electret could statically tune the Fermi level of MoS_2 channel, realizing broad modulation of the initial electrical performance of MoS_2 FET by 2 orders of magnitude through changing the downward prepolarization to upward direction. On the other hand, the external tensile/compressive strain can further enhance/weaken the aligned dipoles in a piezo-electret and result in different piezo-potentials to affect the energy band bending of MoS_2 channel, giving rise to highly sensitive strain sensor (gauge factor ∼4800). The on/off switch was also demonstrated to be fast (0.15 s) and stable (over 1000 s).

DOI: 10.1021/acsnano.8b07477
ACS Nano 2019, 13, 582−590

Under dynamic modulation, the on/off current ratio exceed 4 orders of magnitude with the external strain varying from −0.3% to 0.2%, which was comparable to the device electrical performance under applied gate bias. Notably, the piezo-potential modulation of the light emission of MoS_2 channel was visualized through photoluminescence (PL) spectroscopy. The PL peak of MoS_2 showed a significant blue shift of ∼14 meV when the strain applied on piezo-electret was increased to 1.2%, similar to the MoS_2 light emission control by electric-field gating. Besides, a piezo-electret modulated MoS_2 FET with compact structure design and feasible *in situ* polarization was demonstrated through directly spin-coating a piezo-electret polymer on a MoS_2 channel. Piezoelectric polarization by low-voltage bottom gate pulses (<60 V) enabled comparable modulation effects on the initial transport properties of MoS_2. The proposed static and dynamic piezoelectric modulation of electrical and optical properties in 2D nanomaterials is of great significance in tunable semiconductor devices, sophisticated flexible electronics, highly sensitive mechanical sensors, and human−machine interface.

RESULTS AND DISCUSSION

Figure 1a shows the basis of piezotronics, an emerging field involving piezoelectricity, semiconductor, and photoexcitation. The three-term coupling (among polarization, semiconducting characteristics, and photoexcitation) implies the piezotronic effect on charge carrier transport and separation/recombination at a contact or junction, which promotes the modulation of the energy band levels and optoelectronic process by mechanical stimuli in a dynamic manner. The proposed piezo-electret gated MoS_2 FET further realizes the static modulation of charge transport free from external strain due to the stable remnant potentials in the piezo-electret gate, which complements the three-term coupling and expands a broader application of piezotronics. The schematic illustration of the piezo-electret gated MoS_2 FET is demonstrated in Figure 1b. The uniform and continuous MoS_2 films were grown on sapphire by an oxygen-assisted CVD method to avoid multilayer MoS_2 film deposition.[36] Then the MoS_2 films were transferred to PET substrate with prepatterned Au source−drain electrodes. MoS_2 channel was defined to be 20 μm by standard photolithography and reactive ion etching (RIE). The atomic force microscope (AFM) image of the device demonstrates the monolayer property (∼0.7 nm) of the MoS_2 channel with clean surface (Figure 1c). To enhance the electrostatic field effect on a MoS_2 channel induced by piezo-electret, high-κ Al_2O_3 (30 nm) was selected as the gate dielectric layer by atomic layer deposition (ALD). Indium tin oxide (ITO) was sputtered as an extended gate electrode for capacitive coupling between piezo-electret and MoS_2 FET. Among the piezoelectric polymer family, poly(vinylidenefluoride-*co*-trifluoroethylene) (P(VDF-TrFE)) with VDF content between 50% and 80% presents a preferential ferroelectric β-phase due to the addition of a third fluoride into the TrFE monomer unit, which increased the steric hindrance and induced an all-trans conformation (corresponding to the ferroelectric β-phase).[37] In this work, P(VDF-TrFE) (70/30) was utilized as the piezo-electret to modulate the transport properties of MoS_2 FET through static remnant polarization after poling process and dynamic piezo-potentials under different external strains. The P(VDF-TrFE) film as a top-gate for the device needed to be polarized in advance. The prepolarization rearranged the dipoles in the P(VDF-TrFE) film in an oriented alignment, exhibiting a remanent piezo-potential (the aligned dipoles could be maintained at a certain extent for a long time after removing the external voltage). As shown in Figure 1d, the open circuit voltage produced by P(VDF-TrFE) sandwiched between ITO and Au electrodes shows a linear increment according to the applied strain varied from 0% to 0.5%. In particular, the remanent potential is equivalent to 1.9 V without applying any strains, attributing to the aligned dipole moments after polarization (*i.e.*, positive hydrogen groups and negative fluorine groups conformed in an all-trans ferroelectric β-phase).

Electrical properties of the MoS_2 FET were first characterized by a semiconductor analysis system (Agilent B1500) in atmospheric environment. Typical output curves of MoS_2 FET were shown in Figure 1e. The drain current (I_D) was increased from 0.3 pA to 6.27 μA with a gate voltage increase from −3 to 3 V at a drain voltage (V_D) of 3 V. The linear I−V characteristics at V_D below 1 V demonstrated the good contact between source−drain electrodes and MoS_2 channel. Due to the high dielectric constant of the Al_2O_3, the on/off ratio was nearly 10^5 at low gate voltages sweeping from −3 to 3 V (Figure S1). The mobility was calculated to be ∼30 $cm^2 \cdot V^{-1} \cdot s^{-1}$ with the channel length and width at 20 and 5 μm, respectively. The equivalent circuit of the piezo-electret gated MoS_2 FET is a P(VDF-TrFE) capacitor in series connection with an Al_2O_3 capacitor (Figure S2). Therefore, the charges repelled by the piezo-potential cannot be compensated through the series connection, which imposes an electrostatic field effect on the MoS_2 channel. The equivalent gate bias ($V_{G\text{-}eq}$) under external strains is related to the open circuit voltage ($V_{piezo\text{-}electret}$) produced by the piezo-electret following $V_{G\text{-}eq} = (C_{piezo\text{-}electret}/C_{oxide}) \times V_{piezo\text{-}electret}$, where $C_{piezo\text{-}electret}$ and C_{oxide} are the capacitances of P(VDF-TrFE) and Al_2O_3, respectively. We defined P(VDF-TrFE) without polarization as the pristine state, dipole moments aligned downward as the positive state ($P_{positive}$), and dipole moments aligned upward as the negative state ($P_{negative}$), respectively (Figure S3). After the polarization of P(VDF-TrFE) through applying different polarizing voltages, downward alignment of the dipoles induced an equivalent positive gate bias applied to the MoS_2 channel, which enhanced the electrons in the MoS_2 channel, bent the conduction band of MoS_2 downward, and led to a higher current level compared with the pristine state. In contrast, upward alignment of the dipoles induced an equivalent negative gate bias applied to the MoS_2 channel, which resulted in the conduction band of MoS_2 bending upward and led to a lower current level compared with the pristine state (Figure 1f). Relevant band diagram illustration with opposite prepolarization is shown in the bottom panel of Figure S3. The I_D of MoS_2 FET shows a 2 orders of magnitude variation (V_D = 1 V) under opposite polarization directions. The remanent piezo-potential in the prepolarized piezo-electret film can effectively affect the Fermi level of MoS_2 channel and adjust the current level of the device, which provides an efficient approach to programming the initial electrical performance of the electronic devices for subsequent sophisticated applications.

To verify the equivalent gating effect of piezo-potential, we characterized the optical properties of MoS_2 under different external strains. Different from the top-gate device structure on PET substrate, the monolayer MoS_2 was transferred on SiO_2/

DOI: 10.1021/acsnano.8b07477
ACS Nano 2019, 13, 582−590

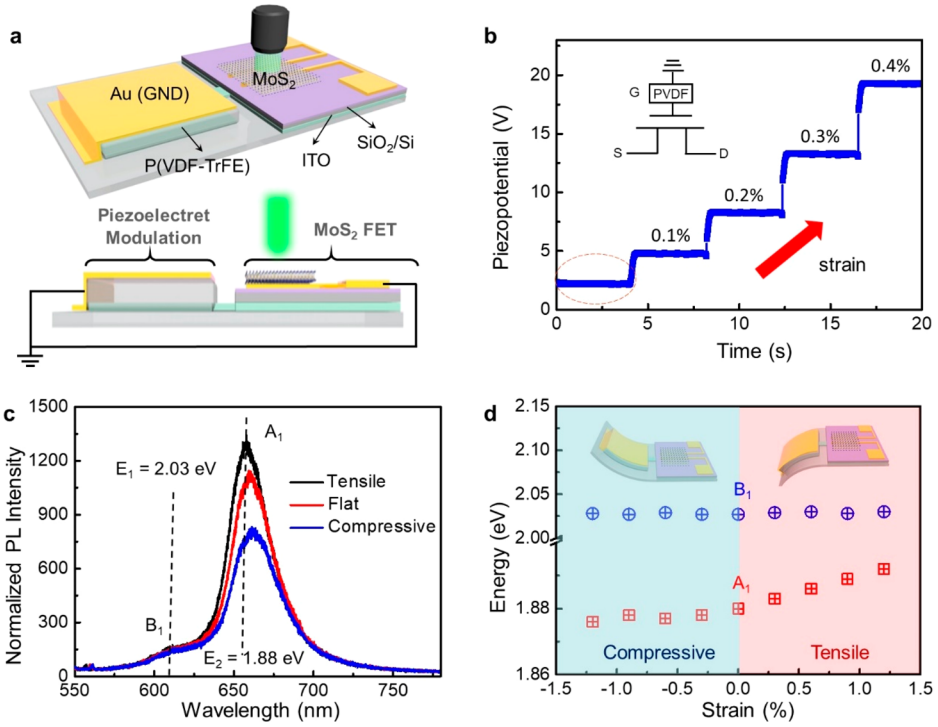

Figure 2. Optical property of MoS_2 gated by the P(VDF-TrFE) film. (a) The schematic illustration of the optical property measurement. (b) The maintainable piezopotential of P(VDF-TrFE) under different strains. (c) The PL spectrum of the MoS_2 FET device with P(VDF-TrFE) device under different strains. (d) Strain-dependent PL peaks position of MoS_2.

Si substrate and modulated by P(VDF-TrFE) through the bottom SiO_2 dielectric to ensure the direct exposure of the MoS_2 surface to the laser (Figure 2a). The detailed structure is shown in Figure S2. The Raman spectrum of MoS_2 without piezo-electret modulation (Figure S4a) confirms the MoS_2 film grown by CVD is monolayer according to the Raman shift at 20 cm^{-1} between two typical Raman peaks: E_{2g} (384 cm^{-1}) and A_{1g} (404 cm^{-1}).[38] In Figure S4b, the two typical PL spectra peaks of the MoS_2 sample are observed at 663 and 613 nm, respectively. These two peaks correspond to the direct optical transitions at the Brillouin zone K-point and the spin−orbital splitting of the valence band, respectively. Therefore, the two resonances corresponding to the energy ∼1.88 eV and ∼2.03 eV are pronounced as A_1 and B_1 excitons.[39,40] Slight red shift of the A_1 peak with our MoS_2 sample compared with the suspended MoS_2 (∼1.90 eV) was mainly caused by the trapped charges doping from substrate.[16]

According to the piezoelectric property of the P(VDF-TrFE), external strains can further enhance/weaken the aligned dipole moments, representing increased/decreased piezopotentials. Figure 2b demonstrates that the open circuit voltages have a stepped increment under increased strains after positive polarization. The PL spectrum of piezo-electret gated MoS_2 FET under tensile/compressive strain is shown in Figure 2c. When the applied strain was increased from −0.2% (compression) to 1.2% (tension), an apparent blue shift of the A_1 excitons (from ∼663 nm to ∼657 nm) with enhanced intensity was observed due to the accumulation of free electrons in monolayer MoS_2. The PL shift was attributed to that the accumulated free electrons by piezopotential alleviated the passivation of MoS_2 surface states deriving from trapped charges at the MoS_2/SiO_2 interfaces, similar to the effect of directly applying positive gate bias.[41] The detailed PL shifts characterized under relevant strains are stable as shown in Figure S5a. The extracted A_1 peaks were observed to represent a blue shift of 14 meV, while the B_1 peak had no obvious change when the strain varied from −1.2% to 1.2% (Figure 2d). The unobvious shift of B_1 peak position under different external strains may be attributed to the mild influence of piezo-potential on the spin−orbital splitting of the MoS_2 valence band. In addition, the intensity of the A_1 peak decreased obviously with the increased strain, further confirming that the piezo-potential effectively alleviated the charge trapping deriving from substrate doping. In Figure S5b, the invariant Raman shift declares that piezo-potential induced by P(VDF-TrFE) has no influence on in-plane vibration and out-of-plane phonon coupling mode of MoS_2. The optical properties of the piezo-electret gated MoS_2 demonstrated that the piezo-potentials induced by external strains were equivalent to gate biases applied to MoS_2 FET.

After investigating the optical properties of MoS_2 imposed by the piezo-potential from P(VDF-TrFE), electrical properties of the piezo-electret gated MoS_2 FET under different strains were characterized in detail. Even though the monolayer MoS_2 had a small piezoelectric output theoretically, the MoS_2 film we grew by CVD method contained some grain boundaries, leading to an ignorable piezoelectric effect from MoS_2 itself. Therefore, the MoS_2 FET without P(VDF-TrFE) regulation had a stable electrical property even under a strain of ∼1%.[18] Due to the piezoelectric property of the polarized P(VDF-TrFE), the piezopotential was linearly proportional to the applied strains (ε) according to $V_{\text{piezo-electret}} = \varepsilon/d$, as illustrated in Figure S6a (d is the piezoelectric coefficient). The induced piezo-potential also represents good stability and long-term durability (Figure S6b,d). As shown in Figure 3a,c, the impositions of tensile and compression strains to the piezo-electret were equivalent to applying positive and negative gate biases to the MoS_2 FET, resulting in corresponding band

DOI: 10.1021/acsnano.8b07477
ACS Nano 2019, 13, 582−590

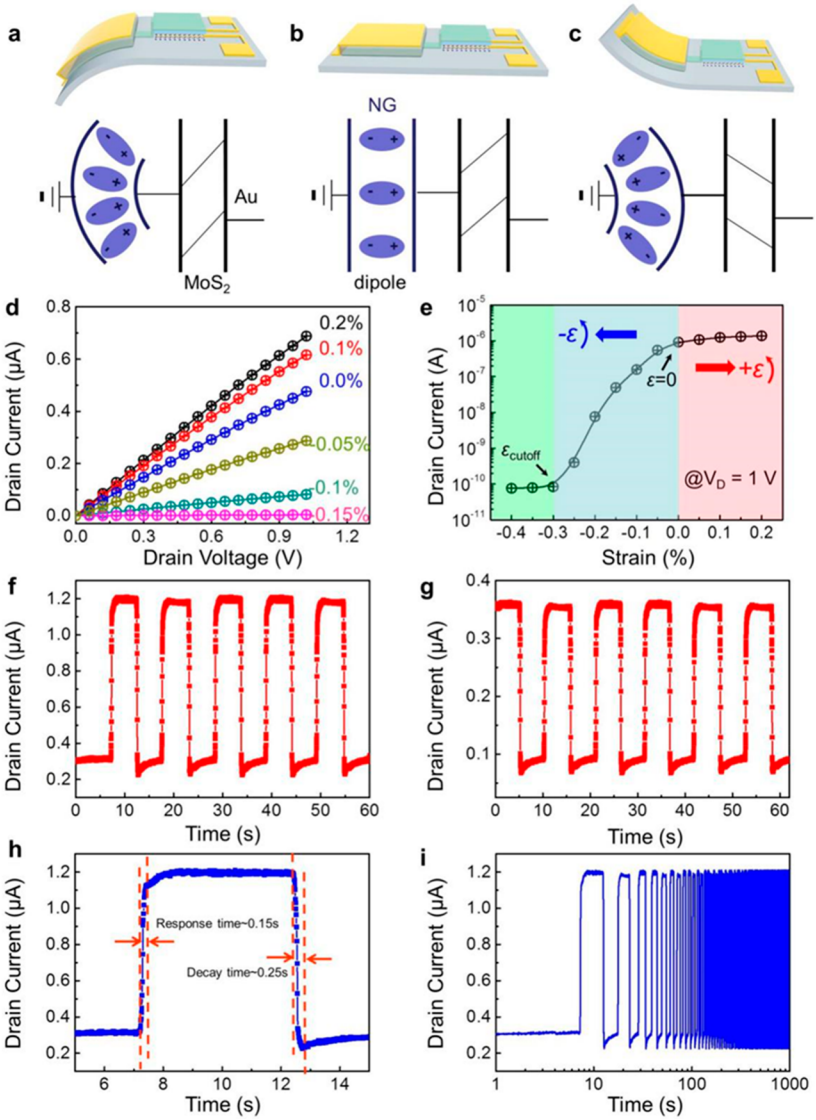

Figure 3. Dynamic electrical regulation of the MoS_2 FET by bending P(VDF-TrFE). (a–c) Corresponding charge distribution of the piezo-electret for tensile, relax, and compression conditions. (d) The output curves of the piezo-electret gated MoS_2 FET under different strains. (e) The transfer curve of piezo-electret gated MoS_2 FET (I_D *vs* ε). (f, g) Dynamic electrical properties of the MoS_2 FET under tensile (0.1%) and compression strain (−0.1%) pulses. (h) Time response of the MoS_2 FET under strain. (i) The stability of MoS_2 FET after 10^3 s measurement.

bends compared with the device in a relax state (Figure 3b). The ineluctable charge trapping from substrate shifted the threshold voltage of MoS_2 FET to the negative direction, giving rise to an enhanced electrons density in the MoS_2 channel (I_D ∼ 0.1 μA) at zero gate bias (Figure S1). To achieve higher on/off ratio of the piezo-electret gated MoS_2 FET, we reasonably polarized P(VDF-TrFE) in the positive state (dipoles moment aligned upward), which induced further accumulation of electrons in MoS_2 (I_D ∼ 1.0 μA, Figure 3e). Thus, applying compressive strain (equivalent to negative gate bias) enabled more capacity to deplete the electrons in MoS_2 channel and realized highly efficient modulation on MoS_2 transport properties. Figure 3d shows the output performance of piezo-electret gated MoS_2 FET. When the strain was increased from −0.15% to 0.2%, the output current of the MoS_2 FET increased from ∼3.8 nA to ∼0.7 μA at V_D = 1 V. The output performance of piezo-electret gated MoS_2 FET with wider V_D sweeping from −3 V to 3 V is shown in Figure S7. The transfer characteristics (I_D *vs* strain) of piezo-electret gated MoS_2 FET is shown in Figure 3e. Through controlling the applied external strain, the device was able to switch from high resistance to low resistance state with I_D varying from 10^{-10} to 10^{-6} A. The on/off ratio tuned by strain was more than 10^4, comparable to the device driven by applied gate voltage in Figure S1. The efficient piezo-potential gating through capacitive coupling was attributed to the high dielectric constant of Al_2O_3 and appropriate static piezo-potential programming on the initial current level of MoS_2 FET. The nonlinear behavior of the output current as a function of strain in Figure 3e was explained as follows: The P(VDF-TrFE) film in positive state (dipoles moments pointing to the ground, Figure 3b) after prepolarization enhanced the electrons in MoS_2 channel, resulting in an increased I_D of 1.0 μA at V_D = 1 V compared with the I_D (∼0.1 μA) of pristine MoS_2 FET in Figure S1. When P(VDF-TrFE) film was subjected to tensile strain (Figure 3a), an enhanced positive

DOI: 10.1021/acsnano.8b07477
ACS Nano 2019, 13, 582–590

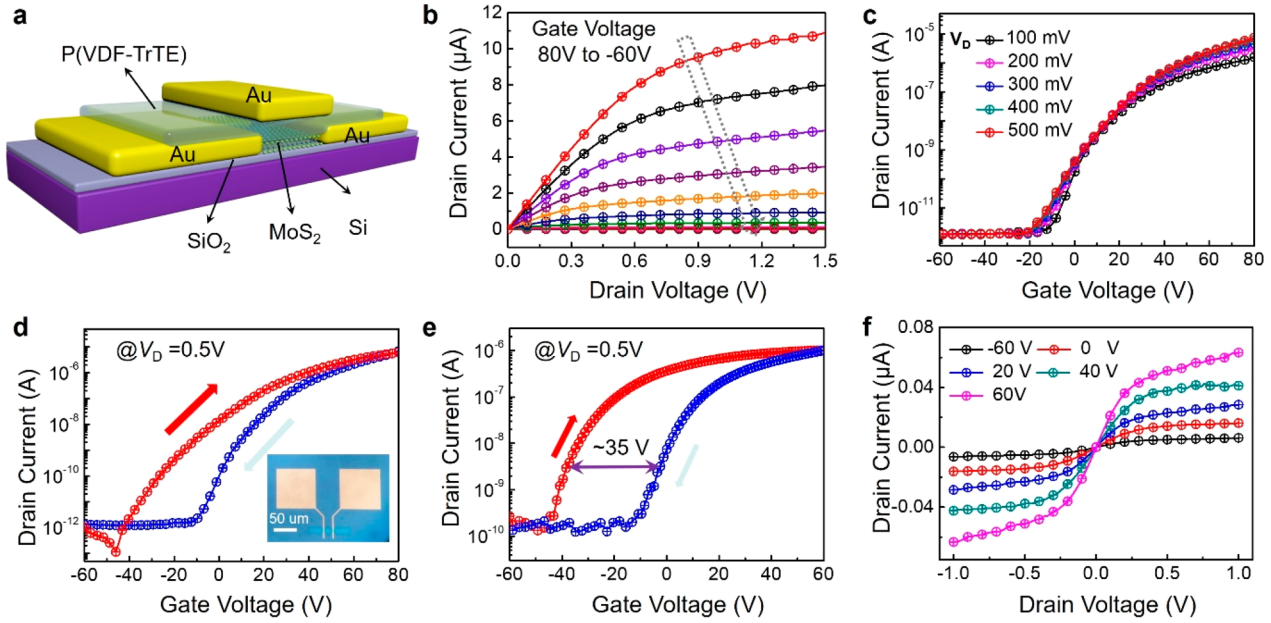

Figure 4. (a) The schematic diagram of the device structure with 300 nm P(VDF-TrFE) covered on top of MoS2 FET. The output curves (b) and transfer curves (c) of the MoS_2 FET on silicon substrate with 300 nm SiO_2. (d) The electrical hysteresis of the device under double sweeps between −60 and 80 V without P(VDF-TrFE) covering. (e) The increased hysteresis of the device after spin-coating piezo-electret on the surface. The scan voltage is the same with (d). (f) The source−drain currents of MoS_2 device after different gate pulses applied to the silicon substrate.

piezo-potential compared with the initial positive state was coupled to MoS_2 FET. It further bent the energy band of MoS_2 downward and led to an increment of I_D from 1.0 μA to 1.1 μA (red region). In contrast, when P(VDF-TrFE) film was subjected to compressive strain (Figure 3c), a negative piezo-potential was coupled to MoS_2 FET. It depleted the electrons in the MoS_2 channel, bent the energy band of MoS_2 upward, and resulted in an exponential decrement of I_D (blue region). When the compressive strain was further increased to −0.3%, enhanced negative piezo-potential was imposed on MoS_2 FET and depleted almost all the free electrons in the MoS_2 channel, resulting in the complete cutoff state of MoS_2 FET (green region). In this region, the I_D was dominated by leakage and charging currents.

As the output currents were associated with the external strain, the piezo-electret gated MoS_2 FET was capable of working as a strain sensor. According to the dramatic resistance change (over 10^4) under applied strains varying from −0.3% to 0.2%, the extracted gauge factor (GF or sensitivity) under compressive strain is 4800 with a strain varying from −0.1% to 0%, while the GF is 250 under a tensile strain from 0% to 0.2% (Figure S8). Notably, the compressive GF achieved in the piezo-electret gated MoS_2 FET strain sensor is much higher than the reported ultrahigh GFs of ZnO tribotronic strain sensors (~1250) and CNT strain sensors (~1000) and far more than the commercial metal foil strain gauges (2−5), p-type germanium strain sensors (~102), or silicon strain sensors (−125−200).[42] The dynamic electrical measurements under tensile (0.1%) and compression (−0.1%) strains show reproducible current switching in Figure 3f,g, respectively (V_D = 1 V). The response and decay time are extracted to be ~0.15 s and ~0.25 s (Figure 3h), which is comparable with other strain sensors based on 2D materials. Long-term stability of the strain sensor (over 1000 s) is also confirmed in Figure 3i. Efficient piezo-potential modulation of the electrical properties demonstrated the great potential of the piezo-electret gated MoS_2 FET as a strain sensor due to the high sensitivity, fast response time, and excellent repeatability.

The demonstrated device architecture occupies extra space due to the piezo-electret patterned on the extended gate. It is important to make a compact design of the piezo-electret gated MoS_2 FET for highly integrated device application. Therefore, preparing a piezo-electret conformal on the FET channel in a vertical structure was proposed to provide an alternative route to piezo-potential modulation. As shown in Figure 4a, the 5 wt % P(VDF-TrFE) was spin-coated on the surface of the MoS_2 device, resulting in a film thickness at ~300 nm (Figure S9). Then 20 nm Au was deposited as a top-gate electrode. The intrinsic piezo-electret (*i.e.*, ferroelectric) characteristic of the P(VDF-TrFE) provided a way to *in situ* tune the electrical property of the device. Before spin-coating P(VDF-TrFE), typical output and transfer performances of MoS_2 FET were first characterized (Figure 4b,c). The on/off ratio and mobility were ~10^6 and ~43 $cm^2 \cdot V^{-1} \cdot s^{-1}$, respectively, comparable to the previous results.[36] A small hysteresis was observed under the bottom gate sweeping in reverse directions from −60 to 80 V (Figure 4d), originating from the substrate doping effect. With the spin-coated P(VDF-TrFE) film on top of the MoS_2 channel, the hysteresis window of the device was enlarged to be 35 V due to the instantaneous polarization switch of P(VDF-TrFE) under forward/backward bottom gate sweeping (Figure 4e). The large hysteresis window indicated the feasibility of polarization switching of the top P(VDF-TrFE) layer through bottom gate bias.

From Figure 4e, it is observed that the MoS_2 channel can be fully accumulated and depleted at gate voltages of 60 V and −60 V, respectively. We reasonably selected pulse voltages at 60 V and −60 V (pulse width at 1 s) as the polarization voltages for the positive and negative states of the P(VDF-TrFE) piezo-electret. The positive/negative pulse voltages set

DOI: 10.1021/acsnano.8b07477
ACS Nano 2019, 13, 582−590

the P(VDF-TrFE) in a persistent positive or negative state due to the remnant piezopotential in the ferroelectric film. Positive polarization (pulse voltage at 60 V) aligned the dipoles in the P(VDF-TrFE) thin film, equivalent to applying a positive top gate to the MoS_2 FET. In contrast, negative polarization (pulse voltage at −60 V) induced an opposite poling electrical field for the P(VDF-TrFE), equivalent to a negative gate bias. The large hysteresis in Figure 4e is attributed to the instantaneous polarization switch of P(VDF-TrTE), confirmed by the similar hysteresis windows in Figure S10 (tested with a MoS_2 FET with 50 nm thickness PMMA interlayer between MoS_2 and P(VDF-TrFE)). This result excluded that the large hysteresis originated from the charge traps at the interface between P(VDF-TrTE) and MoS_2. The P(VDF-TrFE) with top electrode also played a role as a capacitor after back-gate voltage pulse polarization, which could be coupled to the MoS_2 device, leading to the source−drain current change. In addition, to apply polarized voltage from back-gate, the top-gate electrode provided another way to realize the large hysteresis as demonstrated in the previous study.[43] Figure 4f shows the output performance of the compact piezo-electret gated MoS_2 FET. After pulse polarizations from bottom gate, the output currents were statically modulated to increase from 6 nA to 60 nA (V_D at 1 V) without any applied gate voltages or external strains. Similar results with Figure 1f reflected comparable static modulation capacity of the compact piezo-electret gated MoS_2 FET in lower coercive voltage (<60 V). The *in situ* modulation of the electrical property in MoS_2 FET suggests more potential application in highly integrated flexible electronics. In addition, the observed hysteresis window in the piezo-electret gated MoS_2 FET is promising for high-performance nonvolatile memory devices.[44]

CONCLUSION

In conclusion, we successfully demonstrated the piezo-potential modulation of the electron transport properties in MoS_2 FET in both a static and dynamic manner. It offered an efficient way to modulate the Fermi level of the MoS_2 channel without applying gate voltage (over 10^4 on/off switching) and represented great significance in high-performance strain sensors (gauge factor at ∼4800, fast response time of 0.15 s, and good durability over 1000 s). The optical properties of MoS_2 under piezopotetnial modulation were also observed, exhibiting a 14 meV blue shift in the PL peak. The piezo-electret gated MoS_2 FET with compact structure design enabled feasible local polarization to achieve excellent static modulation capacity on MoS_2 channel. The demonstrated static and dynamic coupling between piezo-potential and semiconducting properties was anticipated to enrich the application of piezotronic effect in efficient semiconductor device modulation, tunable sensory systems, highly integrated matrix, and active multifunctional soft electronics.

As we discussed above, the electromechanical piezotronic effect interlinked the mechanical motions with various semiconductor devices, which gave rise to low-power-consuming wearable devices and interactive electronic systems. Besides the accessible mechanical energy in the surrounding environment, thermal energy originating from temperature gradients and fluctuations is ubiquitous in our daily life. The human body itself is a good source of thermal energy. Instead of a piezo-electret, pyroelectric material with ferroelectric phase (pyro-electret) is also promising to integrate with semiconductor devices to realize the static and dynamic pyroelectric modulation. The pyro-potential produced by temperature variation also shows the capacity of tuning the charge carrier transport and separation/recombination.[45] Inspired by the three-term coupling among polarization, semiconductor, and photoexcitation, we suggest the perspective of electrets with piezo-potential, pyro-potential, or combined piezo/pyroelectric potential to couple with nanomaterial-based semiconductor devices (Figure S11). Implemented with the piezo/pyroelectric modulation, the electronics based on an electret may have broader applications in multifunctional sensory systems, highly efficient energy harvesting, human−machine interface, and the Internet of Things (IoT).

METHODS

Materials Preparation. MoS_2 synthesis: The monolayer MoS_2 film was synthesized in a three-temperature-zone CVD system. Sulfur (Alfa Aesar 99.9%) and molybdenum trioxide (MoO_3) (Alfa Aesar 99.999%) were used as precursors and loaded in growth zones I and II, respectively. The 300 nm SiO_2/Si substrate was loaded in zone III. The temperatures of the three temperature zones were 115, 560, and 750 °C, respectively. 100 sccm Argon was used as carrier gas, and the pressure of the system is 1.0 Torr during the synthesis process. For the monolayer MoS_2 growth without defects and multilayer deposition, 0.5 sccm O_2 was bubbled into the tube during the growth process. The whole growth time lasted for 10 min.

Device Fabrication. MoS_2 film was first transferred to PET substrate with predeposited Ti/Au (2 nm/30 nm) source−drain electrodes. Photoresist (AZ5214) was spin-coated on the MoS_2 film at 4000 r/min speed, and the sample was prebaked at 90 °C for 3 min to remove the solvent. Then the UV exposure was performed for 8 s to pattern the MoS_2 channel, and the unnecessary MoS_2 was etched by a reaction ion etching (RIE) system. After using the acetone to remove the protective resist, the 30 nm thickness dielectric layer (Al_2O_3) was deposited by atomic layer deposition (ALD) at 110 °C using Savannah-100 system (Cambridge NanoTech. Inc.). In the ALD process, the precursors were H_2O (heated to 80 °C) and trimethyl aluminum (TMA) (at room temperature), respectively, while the carrier gas was 20 sccm N_2 in high purity. The two precursors were inlet in turn, and the pulse times for TMA and H_2O were 0.015 and 0.15 s, respectively. Every cycle lasted for 40 s, and the thickness of the layer increased ∼0.9 Å. Then 20 nm ITO was deposited as the top-gate and extended electrode for piezo-electret. The P(VDF-TrFE) was precisely spin-coated on the extended ITO electrode with a polymer stencil. After prepolarization, 30 nm Au was deposited as the top electrode. For the compact piezo-electret gated MoS_2 FET, after patterning the MoS_2 channel and source−drain electrodes, 5% P(VDF-TrFE) dissolved in dimethylformamide (DMF) was spin coated on the device surface at 3000 r/min for 1 min and then baked at 140 °C for 4 h to improve its crystallization. The achieved P(VDF-TrFE) ferroelectric film thickness was ∼300 nm. Then the top gate electrodes (30 nm Au) were deposited followed by photolithography, and the ethylic acid was used in the lift-off process.

Characterization. Raman and PL measurement: The Raman shift and PL measurements were performed on a JY Horiba HR800 system. The wavelength of emission laser is 532 nm (spot size ∼1 μm, power ∼1 mW). The MoS_2 FET was placed in a chip-carrier in the chamber and wire-bonded to the external measurement equipment. To achieve a long working distance, a 50× objective lens was used for laser focusing and signal collecting. The strain applied on the P(VDF-TrFE) piezo-electret was supplied with a motorized positioning system. Under each strain condition, more than 20 spots were measured for both Raman and PL spectra to reduce the measurement errors. The strain on P(VDF-TrFE) device was applied by a motorized positioning system. The detailed strain calculation followed: $\varepsilon = \frac{\Delta L}{L_0} = \frac{(\Delta t + R)\theta - R\theta}{R\theta} = \frac{\Delta t}{R}$, where L_0 and L are the original and strained length of the substrate, Δt and R are half

DOI: 10.1021/acsnano.8b07477
ACS Nano 2019, 13, 582−590

thickness and curvature of the substrate, respectively. All the measurements of MoS_2 FET electrical property gated by P(VDF-TrFE) were performed with a semiconductor analysis system (Agilent 1500A) under ambient conditions.

ASSOCIATED CONTENT

Supporting Information

The Supporting Information is available free of charge on the ACS Publications website at DOI: 10.1021/acsnano.8b07477.

Transfer property of MoS_2 FET without P(VDF-TrFE); schematic diagram of the device back-gated by the P(VDF-TrFE); energy band bend and charge distribution in P(VDF-TrFE) with different polarization conditions; Raman shift and PL spectrum for the pristine MoS_2 film on SiO_2 substrate by CVD growth; Raman shift and PL spectrum for monolayer MoS_2 FET with P(VDF-TrFE) as gate material under different strains; piezoelectrical property of the P(VDF-TrFE) device; output property of MoS_2 FET changed with the strain applied on the P(VDF-TrFE) film; gauge factor of the piezo-electret gate MoS_2 FET strain sensor; measurement of the thickness of P(VDF-TrFE) spin-coated on MoS_2 film; hysteresis of the device with PMMA as an interlayer; perspective of a research direction and applications with piezo- and pyro-electrets (PDF)

AUTHOR INFORMATION

Corresponding Authors

*E-mail: sunqijun@binn.cas.cn.
*E-mail: zhong.wang@mse.gatech.edu.
*E-mail: gyzhang@iphy.ac.cn.

ORCID

Qijun Sun: 0000-0003-2130-7389
Zhong Lin Wang: 0000-0002-5530-0380

Notes

The authors declare no competing financial interest.

ACKNOWLEDGMENTS

This work is financially supported by the National Key Research and Development Program of China (2016YFA0202703, 2016YFA0202704), National Natural Science Foundation of China (61804009, 51605034, 51711540300), Beijing Natural Science Foundation (4184111), the "Hundred Talents Program" of the Chinese Academy of Science and State Key Laboratory of Precision Measuring Technology and Instruments (Tianjin University). G.Z. thanks the National Key R&D program (grant no. 2016YFA0300904), the National Science Foundation of China (NSFC, grant no. 61325021), the Key Research Program of Frontier Sciences, CAS (grant no. QYZDB-SSW-SLH004), and the Strategic Priority Research Program (B) of the Chinese Academy of Sciences (grant no. XDB07010100) for financial support.

REFERENCES

(1) Wu, W. Z.; Wang, Z. L. Piezotronics and Piezo-Phototronics for Adaptive Electronics and Optoelectronics. *Nat. Rev. Mater.* **2016**, *1*, 16031.
(2) Wang, Z. L.; Wu, W. Z. Piezotronics and Piezo-Phototronics: Fundamentals and Applications. *Natl. Sci. Rev.* **2014**, *1*, 62−90.
(3) Liu, W.; Lee, M.; Ding, L.; Liu, J.; Wang, Z. L. Piezopotential Gated Nanowire-Nanotube Hybrid Field-Effect Transistor. *Nano Lett.* **2010**, *10*, 3084−3089.
(4) Wu, W.; Wen, X.; Wang, Z. L. Taxel-Addressable Matrix of Vertical-Nanowire Piezotronic Transistors for Active/Adaptive Tactile Imaging. *Science* **2013**, *340*, 952−957.
(5) Wang, Z. L.; Song, J. H. Piezoelectric Nanogenerators Based on Zinc Oxide Nanowire Arrays. *Science* **2006**, *312*, 242−246.
(6) Pan, C.; Dong, L.; Zhu, G.; Niu, S.; Yu, R.; Yang, Q.; Liu, Y.; Wang, Z. L. High-Resolution Electroluminescent Imaging of Pressure Distribution Using a Piezoelectric Nanowire LED Array. *Nat. Photonics* **2013**, *7*, 752−758.
(7) Wang, Z. L. Self-Powered Nanosensors and Nanosystems. *Adv. Mater.* **2012**, *24*, 280−285.
(8) Wang, Z. L. Toward Self-Powered Sensor Networks. *Nano Today* **2010**, *5*, 512−514.
(9) Takei, K.; Takahashi, T.; Ho, J. C.; Ko, H.; Gillies, A. G.; Leu, P. W.; Fearing, R. S.; Javey, A. Nanowire Active-Matrix Circuitry for Low-Voltage Macroscale Artificial Skin. *Nat. Mater.* **2010**, *9*, 821−826.
(10) Wang, C.; Hwang, D.; Yu, Z. B.; Takei, K.; Park, J.; Chen, T.; Ma, B. W.; Javey, A. User-Interactive Electronic Skin for Instantaneous Pressure Visualization. *Nat. Mater.* **2013**, *12*, 899−904.
(11) Radisavljevic, B.; Radenovic, A.; Brivio, J.; Giacometti, V.; Kis, A. Single-Layer MoS_2 Transistors. *Nat. Nanotechnol.* **2011**, *6*, 147−150.
(12) Brivio, J.; Alexander, D. T. L.; Kis, A. Ripples and Layers in Ultrathin MoS_2 Membranes. *Nano Lett.* **2011**, *11*, 5148−5153.
(13) Larentis, S.; Fallahazad, B.; Tutuc, E. Field-Effect Transistors and Intrinsic Mobility in Ultra-Thin $MoSe_2$ Layers. *Appl. Phys. Lett.* **2012**, *101*, 223104.
(14) Wang, Q. H.; Kalantar-Zadeh, K.; Kis, A.; Coleman, J. N.; Strano, M. S. Electronics and Optoelectronics of Two-Dimensional Transition Metal Dichalcogenides. *Nat. Nanotechnol.* **2012**, *7*, 699−712.
(15) Das, S.; Appenzeller, J. WSe_2 Field Effect Transistors with Enhanced Ambipolar Characteristics. *Appl. Phys. Lett.* **2013**, *103*, 103501.
(16) Mak, K. F.; Lee, C.; Hone, J.; Shan, J.; Heinz, T. F. Atomically Thin MoS_2: A New Direct-Gap Semiconductor. *Phys. Rev. Lett.* **2010**, *105*, 136805.
(17) Cui, X.; Lee, G. H.; Kim, Y. D.; Arefe, G.; Huang, P. Y.; Lee, C. H.; Chenet, D. A.; Zhang, X.; Wang, L.; Ye, F.; Pizzocchero, F.; Jessen, B. S.; Watanabe, K.; Taniguchi, T.; Muller, D. A.; Low, T.; Kim, P.; Hone, J. Multi-Terminal Transport Measurements of MoS_2 Using a Van der Waals Heterostructure Device Platform. *Nat. Nanotechnol.* **2015**, *10*, 534−540.
(18) Zhao, J.; Chen, W.; Meng, J. L.; Yu, H.; Liao, M. Z.; Zhu, J. Q.; Yang, R.; Shi, D. X.; Zhang, G. Y. Integrated Flexible and High-Quality Thin Film Transistors Based on Monolayer MoS_2. Adv. *Electron. Mater.* **2016**, *2*, 1500379.
(19) Xie, L.; Liao, M. Z.; Wang, S. P.; Yu, H.; Du, L. J.; Tang, J.; Zhao, J.; Zhang, J.; Chen, P.; Lu, X. B.; Wang, G. L.; Xie, G. B.; Yang, R.; Shi, D. X.; Zhang, G. Y. Graphene-Contacted Ultrashort Channel Monolayer MoS_2 Transistors. *Adv. Mater.* **2017**, *29*, 1702522.
(20) Zhao, J.; Li, N.; Yu, H.; Wei, Z.; Liao, M. Z.; Chen, P.; Wang, S. P.; Shi, D. X.; Zhang, G. Y. Highly Sensitive MoS_2 Humidity Sensors Array for Noncontact Sensation. *Adv. Mater.* **2017**, *29*, 1702076.
(21) Wang, H.; Yu, L. L.; Lee, Y. H.; Shi, Y. M.; Hsu, A.; Chin, M. L.; Li, L. J.; Dubey, M.; Kong, J.; Palacios, T. Integrated Circuits Based on Bilayer MoS_2 Transistors. *Nano Lett.* **2012**, *12*, 4674.
(22) Pu, J.; Yomogida, Y.; Liu, K. K.; Li, L. J.; Iwasa, Y.; Takenobu, T. Highly Flexible MoS_2 Thin-Film Transistors with Ion Gel Dielectrics. *Nano Lett.* **2012**, *12*, 4013−4017.
(23) Roy, T.; Tosun, M.; Kang, J. S.; Sachid, A. B.; Desai, S. B.; Hettick, M.; Hu, C. M. C.; Javey, A. Field-Effect Transistors Built from All Two-Dimensional Material Components. *ACS Nano* **2014**, *8*, 6259−6264.

DOI: 10.1021/acsnano.8b07477
ACS Nano 2019, 13, 582−590

(24) Zhang, X. K.; Liao, Q. L.; Liu, S.; Kang, Z.; Zhang, Z.; Du, J. L.; Li, F.; Zhang, S. H.; Xiao, J. K.; Liu, B.; Ou, Y.; Liu, X. Z.; Gu, L.; Zhang, Y. Poly(4-styrenesulfonate)-Induced Sulfur Vacancy Self-Healing Strategy for Monolayer MoS_2 Homojunction Photodiode. *Nat. Commun.* **2017**, *8*, 15881.
(25) Wu, H. L.; Kang, Z.; Zhang, Z. H.; Zhang, Z.; Si, H. N.; Liao, Q. L.; Zhang, S. C.; Wu, J.; Zhang, X. K.; Zhang, Y. Interfacial Charge Behavior Modulation in Perovskite Quantum Dot-Monolayer MoS_2 0D-2D Mixed-Dimensional Van der Waals Heterostructures. *Adv. Funct. Mater.* **2018**, *28*, 1802015.
(26) Wu, W. Z.; Wang, L.; Li, Y. L.; Zhang, F.; Lin, L.; Niu, S. M.; Chenet, D.; Zhang, X.; Hao, Y. F.; Heinz, T. F.; Hone, J.; Wang, Z. L. Piezoelectricity of Single-Atomic-Layer MoS_2 for Energy Conversion and Piezotronics. *Nature* **2014**, *514*, 470−474.
(27) Qi, J.; Lan, Y.; Stieg, A. Z.; Chen, J.; Zhong, Y.; Li, L.; Chen, C.; Zhang, Y.; Wang, K. L. Piezoelectric Effect in Chemical Vapour Deposition-Grown Atomic-Monolayer Triangular Molybdenum Disulfide Piezotronics. *Nat. Commun.* **2015**, *6*, 7430.
(28) Liu, J.; Goswami, A.; Jiang, K.; Khan, F.; Kim, S.; McGee, R.; Li, Z.; Hu, Z. Y.; Lee, J. C.; Thundat, T. Direct-Current Triboelectricity Generation by a Sliding Schottky Nanocontact on MoS_2 Multilayers. *Nat. Nanotechnol.* **2018**, *13*, 112−116.
(29) Sun, Q.; Seung, W.; Kim, B. J.; Seo, S.; Kim, S.; Cho, J. H. Active Matrix Electronic Skin Strain Sensor Based on Piezopotential-Powered Graphene Transistors. *Adv. Mater.* **2015**, *27*, 3411−3417.
(30) Kim, S.; Choi, Y. J.; Woo, H. J.; Sun, Q.; Lee, S.; Kang, M. S.; Song, Y. J.; Wang, Z. L.; Cho, J. H. Piezotronic Graphene Barristor: Efficient and Interactive Modulation of Schottky Barrier. *Nano Energy* **2018**, *50*, 598−605.
(31) Sun, Q.; Ho, D. H.; Choi, Y.; Pan, C.; Kim, D. H.; Wang, Z. L.; Cho, J. H. Piezopotential-Programmed Multilevel Nonvolatile Memory As Triggered by Mechanical Stimuli. *ACS Nano* **2016**, *10*, 11037−11043.
(32) Persano, L.; Dagdeviren, C.; Su, Y.; Zhang, Y.; Girardo, S.; Pisignano, D.; Huang, Y.; Rogers, J. A. High Performance Piezoelectric Devices Based on Aligned Arrays of Nanofibers of Poly (vinylidenefluoride-co-trifluoroethylene). *Nat. Commun.* **2013**, *4*, 1633.
(33) Bauer, S. Piezo-, pyro- and ferroelectrets: Soft Transducer Materials for Electromechanical Energy Conversion. *IEEE Trans. Dielectr. Electr. Insul.* **2006**, *13*, 953−962.
(34) Okada, K.; Yasufuku, H.; et al. Electrode Structures in Diode-Type Cadmium Telluride Detectors: Field Emission Scanning Electron Microscopy and Energy-Dispersive X-Ray Microanalysis. *Appl. Phys. Lett.* **2008**, *92*, 073501.
(35) Yang, Y.; Zhang, H. L.; Zhong, X. D.; Yi, F.; Yu, R. M.; Zhang, Y.; Wang, Z. L. Electret Film-Enhanced Triboelectric Nanogenerator Matrix for Self-Powered Instantaneous Tactile Imaging. *ACS Appl. Mater. Interfaces* **2014**, *6*, 3680−3688.
(36) Chen, W.; Zhao, J.; Zhang, J.; Gu, L.; Yang, Z. Z.; Li, X. M.; Yu, H.; Zhu, X. T.; Yang, R.; Shi, D. X.; Lin, X. C.; Guo, J. D.; Bai, X. D.; Zhang, G. Y. Oxygen-Assisted Chemical Vapor Deposition Growth of Large Single-Crystal and High-Quality Monolayer MoS_2. *J. Am. Chem. Soc.* **2015**, *137*, 15632−15635.
(37) Ruan, L. X.; Yao, X. N.; Chang, Y. F.; Zhou, L. Q.; Qin, G. W.; Zhang, X. M. Properties and Applications of the β Phase Poly (vinylidene fluoride). *Polymers* **2018**, *10*, 228.
(38) Lee, C.; Yan, H.; Brus, L. E.; Heinz, T. F.; Hone, J.; Ryu, S. Anomalous Lattice Vibrations of Single- and Few-Layer MoS_2. *ACS Nano* **2010**, *4*, 2695−2700.
(39) Mak, K. F.; He, K. L.; Lee, C.; Lee, G. H.; Hone, J.; Heinz, T. F.; Shan, J. Tightly Bound Trions in Monolayer MoS_2. *Nat. Mater.* **2013**, *12*, 207−211.
(40) Splendiani, A.; Sun, L.; Zhang, Y. B.; Li, T. S.; Kim, J.; Chim, C. Y.; Galli, G.; Wang, F. Emerging Photoluminescence in Monolayer MoS_2. *Nano Lett.* **2010**, *10*, 1271−1275.
(41) Li, Z.; Chang, S.; Chen, C.; Cronin, S. B. Enhanced Photocurrent and Photoluminescence Spectra in MoS_2 Under Ionic Liquid Gating. *Nano Res.* **2014**, *7*, 973−980.
(42) Zhou, J.; Gu, Y.; Fei, P.; Mai, W.; Gao, Y.; Yang, R.; Bao, G.; Wang, Z. L. Flexible Piezotronic Strain Sensor. *Nano Lett.* **2008**, *8*, 3035−3040.
(43) Lee, H. S.; Min, S. W.; Park, M. K.; Lee, Y. T.; Jeon, P. J.; Kim, J. H.; Ryu, S.; Im, S. MoS_2 Nanosheets for Top-Gate Nonvolatile Memory Transistor Channel. *Small* **2012**, *8*, 3111−3115.
(44) Wang, X. D.; Wang, P.; Wang, J. L.; Hu, W. D.; Zhou, X. H.; Guo, N.; Huang, H.; Sun, S.; Shen, H.; Lin, T.; Tang, M. H.; Liao, L.; Jiang, A. Q.; Sun, J. L.; Meng, X. J.; Chen, X. S.; Lu, W.; Chu, J. H. Ultrasensitive and Broadband MoS_2 Photodetector Driven by Ferroelectrics. *Adv. Mater.* **2015**, *27*, 6575−6581.
(45) Zhang, K.; Wang, Z. L.; Yang, Y. Enhanced P3HT/ZnO Nanowire Array Solar Cells by Pyro-Phototronic Effect. *ACS Nano* **2016**, *10*, 10331−10338.

DOI: 10.1021/acsnano.8b07477
ACS Nano 2019, 13, 582−590